Optical dressing of the electronic response of two-dimensional semiconductors in quantum and classical descriptions of cavity electrodynamics

Ivan Amelio,[1,2] Lukas Korosec,[3] Iacopo Carusotto,[2] and Giacomo Mazza[3,*]
[1]*Institute of Quantum Electronics ETH Zurich, CH-8093 Zurich, Switzerland*
[2]*INO-CNR BEC Center and Dipartimento di Fisica, Università di Trento, 38123 Povo, Italy*
[3]*DQMP, Université de Genève, 24 quai Ernest Ansermet, CH-1211 Genève, Switzerland*

(Received 11 June 2021; revised 8 November 2021; accepted 30 November 2021; published 9 December 2021)

We study quantum effects of the vacuum light-matter interaction in materials embedded in optical cavities. We focus on the electronic response of a two-dimensional semiconductor placed inside a planar cavity. By using a diagrammatic expansion of the electron-photon interaction, we describe signatures of light-matter hybridization characterized by large asymmetric shifts of the spectral weight at resonant frequencies. We follow the evolution of the light dressing from the cavity to the free-space limit. In the cavity limit, light-matter hybridization results in a modification of the optical gap with sizable spectral weight appearing below the bare gap edge. In the limit of large cavities, we find a residual redistribution of spectral weight which becomes independent of the distance between the two mirrors. We show that the photon dressing of the electronic response can be fully explained by using a classical description of light. The classical description is found to hold up to a strong coupling regime of the light-matter interaction highlighted by the large modification of the photon spectra with respect to the empty cavity. We show that, despite the strong coupling, quantum corrections are negligibly small and weakly dependent on the cavity confinement. As a consequence, in contrast to the optical gap, the single-particle electronic band gap is not sensibly modified by strong coupling. Our results show that quantum corrections are dominated by off-resonant photon modes at high energy. As such, cavity confinement can hardly be seen as a knob to control the quantum effects of the light-matter interaction in vacuum.

DOI: 10.1103/PhysRevB.104.235120

I. INTRODUCTION

The interaction of light and matter in vacuum conditions, i.e., in the absence of driving fields, has been proposed as an advanced frontier for the control of matter properties [1]. In this perspective, electromagnetic environments capable of confining light over small volumes, namely cavities, play a fundamental role.

The spatial confinement can enhance fluctuations of electromagnetic fields and in turn result in a significant increase of the strength of the vacuum light-matter interaction. These effects become manifest in the so-called strong and ultrastrong coupling regimes of light-matter interaction in which matter and light degrees of freedom mix and form strongly intertwined excitations known as polaritons [2,3].

Recently, several proposals have suggested light-matter hybridization as a novel tool to control emergent macroscopic phenomena, such as superconductivity, ferroelectricity and magnetic or topological phases by embedding so-called quantum materials in such electromagnetic environments [4–17]. The general idea is that when a material is embedded inside a cavity, interaction effects due to vacuum quantum fluctuations of the electromagnetic fields become strong enough to induce major modifications of the ground state properties of the material. The new perspective has been termed the quantum route towards the light manipulation of matter [18,19], as opposed to the classical approach which instead relies on the stimulation of matter by means of coherent driving fields [20–22]. The main difference between the two approaches can be traced back to the different roles played by the photonic degrees of freedom in the dynamics of the coupled light-matter system. In the classical regime, the driving field contains a macroscopically large number of photons whose dynamics is assumed to be entirely determined by external sources. In contrast, in the quantum case vacuum photons are considered to be active degrees of freedom whose dynamics is self-consistently determined by the coupling with the matter microscopic excitations as described in the framework of the nonrelativistic quantum electrodynamics (QED).

Despite this conceptual distinction, the differences between the two regimes of the light-matter interaction can be, in reality, much less sharply defined. Indeed, as originally pointed out in a seminal work by Jaynes and Cummings [23], semiclassical approaches based on Maxwell's equations can be extremely effective in describing light-matter coupling down to the vacuum limit. At the same time, even in the presence of coherent driving fields, the feedback of internal sources onto driving photons can play an important role as recently discussed in the context of light-stimulated strongly correlated electron systems [24].

In this context, a deeper understanding of the crossover between quantum and classical regimes of the light-matter interactions as a function of the environment represents a fundamental step towards practical cavity applications of solid-state materials [25]. General open questions concern, for

*giacomo.mazza@unige.ch

example, the effectiveness of the coupling in the modification of the ground state properties of a material and how these effects depend on the resonance conditions between multiple matter excitations and the electromagnetic modes of the environment.

In this paper, we address these questions by analyzing the effects of light-matter hybridization on the electronic response of a two-dimensional semiconductor embedded in a planar cavity. Photon dressing of the dc electronic transport properties has been recently discussed in the context of organic semiconductors [26–28] and two-dimensional electron gases [29–31]. These descriptions usually rely on effective models in which the effect of the cavity is incorporated as effective coupling strengths. Here we consider a multimode electron-photon Hamiltonian for which, at fixed electronic structure of the material, the light-matter interaction is entirely controlled by the distance between the mirrors. This allows us to follow the evolution of the light dressing from the *cavity limit*, characterized by a strong light confinement, to the *free-space limit*, in which effects of the light-matter interaction become independent of the environment.

By making use of a diagrammatic expansion of the electron-photon interaction, we show sharp redistributions of spectral weight in the frequency dependent conductivity due to the hybridization of resonant modes with the continuum of electronic excitations in the material. The shift results in a modification of the optical gap which smoothly evolves into a residual subgap redistribution of the spectral weight persisting up to the free-space limit. We rationalize the results of the diagrammatic expansion in terms of a semiclassical description of the vacuum fluctuations in which classical electromagnetic fields are sourced by current fluctuations in the material. By comparing the two approaches, we show that the classical description exactly reproduces the results of the diagrammatic expansion in the Gaussian approximation up to the strong coupling limit.

We estimate the size of quantum effects by computing corrections beyond the Gaussian approximation. We show that, because of the small photon density of states at low energies, quantum corrections are expected to be negligibly small and dominated by off-resonant modes at high energy. Therefore quantum corrections are weakly dependent on the cavity confinement. The direct consequence of our results is that, while the optical gap, described by the current-current response function, is sensibly modified by the optical dressing in the cavity, the electronic band gap, determined by the single-particle electronic Greens' function, remains unchanged.

We organize the paper as follows. In Sec. II, we present the setup studied in this work. Section III reports the detail of the linear response theory and the diagrammatic expansion. In Sec. IV, we present main results concerning signatures of the light-matter hybridization in the conductivity. Eventually, in Sec. V, we address the comparison between the classical description and the quantum theory.

II. THEORETICAL FRAMEWORK

The theoretical framework used in this work is specified by the cavity, the electronic system, and the interaction Hamiltonian.

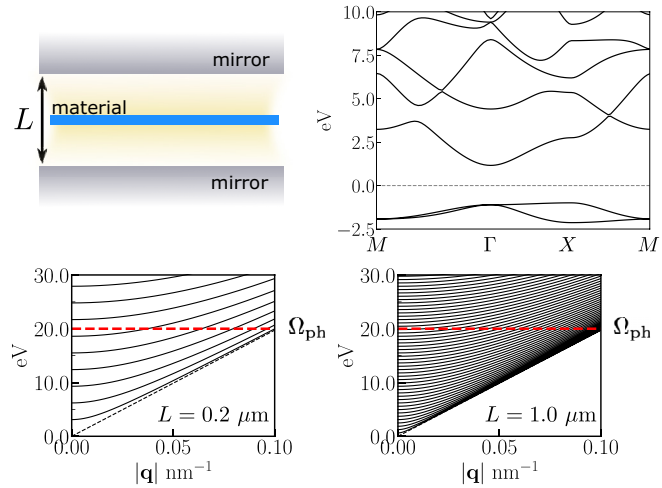

FIG. 1. (Top left) Sketch of a two-dimensional material placed between two perfectly conducting mirrors separated by a distance L. (Top right) Electronic bands of the two-dimensional system as obtained by using the periodic potential defined by the parameters $v_0 = 5.0$ eV, $\lambda = 0.2$ nm^{-1}, $\alpha = 2$, and $\xi = 0.1$ nm, see text. (Bottom) Photon dispersions for two cavity lengths. Red dashed line indicate a photon cutoff used in the calculations. The massless mode drawn with a dashed line represents the mode with zero in-plane component.

A. Cavity

We consider a two-dimensional material placed in the center of a planar cavity made by two parallel perfectly conducting mirrors separated by a distance L, see Fig. 1. Following Ref. [32], the quantization of the electromagnetic field in the planar geometry leads to the expansion of the vector potential operator

$$\mathbf{A}(\mathbf{x}, z) = \sum_{\mathbf{q}q_z\sigma} \frac{\gamma_{\mathbf{q}q_z}}{\sqrt{V}} \left(\boldsymbol{w}_{\mathbf{q}q_z\sigma}(\mathbf{x}, z) a^\dagger_{\mathbf{q}q_z\sigma} + \text{H.c.} \right), \tag{1}$$

where $a^\dagger_{\mathbf{q}q_z\sigma}$ are creation operators of photons with in-plane momentum $\mathbf{q}$, out-of-plane momentum q_z and polarization σ. The amplitudes $\gamma_{\mathbf{q}q_z} \equiv \sqrt{\frac{\hbar^2}{2\epsilon_0 \omega_{\mathbf{q}q_z}}}$ depends on the energy of the photon modes $\omega_{\mathbf{q}q_z} \equiv \hbar c \sqrt{\mathbf{q}^2 + q_z^2}$. In the rest of the paper, we will measure all the frequencies in energy units by incorporating the $\hbar$ in the definition of frequency. $V = S \times L$ is the cavity volume, being S the area of the mirrors, which is assumed to be equal to that of the embedded material. Eventually we will take the thermodynamic limit, by sending $S \to \infty$ and keeping the density of electrons in the material fixed. As a consequence, $\mathbf{q}$ is described by a continuous variable in the (q_x, q_y) plane, whereas q_z is quantized as $q_z = \frac{\pi}{L} n$, with n a positive integer. Dispersion of the modes for two cavity lengths are reported in Fig. 1.

The mode functions $\boldsymbol{w}_{\mathbf{q}q_z\sigma}(\mathbf{x}, z) \equiv e^{i\mathbf{q}\mathbf{x}} \boldsymbol{v}_{\mathbf{q}q_z\sigma}(z)$ are determined by imposing the boundary conditions at the mirrors $\mathbf{E}_\parallel(\mathbf{x}, z = 0) = \mathbf{E}_\parallel(\mathbf{x}, z = L) = 0$, $\mathbf{B}_\perp(\mathbf{x}, z = 0) = \mathbf{B}_\perp(\mathbf{x}, z = L) = 0$ and the transversality condition $\nabla \cdot \mathbf{A} = 0$. For each momentum $(\mathbf{q}, q_z)$, there exist two orthogonal polarizations $\boldsymbol{w}_{\mathbf{q}q_z\sigma} \cdot \boldsymbol{w}_{\mathbf{q}q_z\sigma'} \propto \delta_{\sigma\sigma'}$. The mode functions are specified by the

vectors $\boldsymbol{v}_{\mathbf{q}q_z\sigma}(z)$ which depend on the momenta and polarization [32].

B. Electrons

We model the electronic properties of the material by considering a two-dimensional periodic potential on a square lattice with lattice parameter $a = 0.5$ nm. The periodic potential is defined by $V_{\text{periodic}}(\mathbf{x}) = \sum_{\mathbf{R}} v(\mathbf{x} - \mathbf{R})$ where the sum extends over all the points in the Bravais lattice and $v(\mathbf{x})$ represents a deep potential well centered in the middle of the square unit cell mimicking an atomic center. We define the atomic-like potential as $v(\mathbf{x}) = -v_0 \exp(-\lambda|\mathbf{x}|)/(|\mathbf{x}|^\alpha + \xi^\alpha)$. The parameters v_0, λ, α and η are chosen in order to get a band structure with bandwidths of the order of the eV, see Fig. 1.

We tune the chemical potential in the middle of the band gap. The size of the indirect band gap is $\sim$2 eV, slightly smaller than the direct optical gap at the Γ point $\sim$2.25 eV. The details of the band structure, as for example the fact that the electronic gap is slightly indirect, do not affect in any qualitative way the results presented in this paper.

The main goal of this paper is to estimate the effects of hybridization of matter and transverse photons. As such we do not consider the effects of the electron-electron interactions as well as effects on the screening of the Coulomb interaction due to the image charges on the mirrors [10,33]. Throughout the paper the electron-photon interaction represents the only source of scattering. We also consider the electrons spinless.

C. Multimode QED Hamiltonian

The electron-photon interaction is introduced by the minimal coupling $\mathbf{p} \to \mathbf{p} + e\mathbf{A}(\mathbf{x})$,

$$H = H_0 + \int d\mathbf{x}\ \Psi^\dagger(\mathbf{x}) \frac{(\mathbf{p} + e\mathbf{A}(\mathbf{x}))^2}{2m} \Psi(\mathbf{x}) + \int d\mathbf{x}\ \Psi^\dagger(\mathbf{x}) V_{\text{periodic}}(\mathbf{x}) \Psi(\mathbf{x}), \tag{2}$$

where $\mathbf{A}(\mathbf{x}) \equiv \mathbf{A}(\mathbf{x}, z = L/2)$ is the vector potential operator evaluated in the middle of the cavity. The fermionic fields $\Psi(\mathbf{x}) = \sum_{\mathbf{k}\nu} \varphi_{\mathbf{k}\nu}(\mathbf{x}) c_{\mathbf{k}\nu}$ are expanded onto the complete set of Bloch wave functions $\varphi_{\mathbf{k}\nu}(\mathbf{x})$ of the two-dimensional periodic potential. $H_0 = \frac{1}{2}\int d\mathbf{x}dz\ \varepsilon_0 \mathbf{E}^2(\mathbf{x}, z) + \frac{1}{\mu_0}\mathbf{B}^2(\mathbf{x}, z) = \sum_Q \omega_Q a_Q^\dagger a_Q$ is the total energy of the electromagnetic field inside the cavity. In the last expansion, we used the compact notation $Q \equiv (\mathbf{q}, q_z, \sigma)$. Expansion of the Hamiltonian gives

$$H = \sum_Q \omega_Q a_Q^\dagger a_Q + \sum_{\mathbf{k}\nu} \varepsilon_{\mathbf{k}\nu} c_{\mathbf{k}\nu}^\dagger c_{\mathbf{k}\nu} + H_{AP} + H_{AA} \tag{3}$$

with

$$H_{AP} = \frac{e}{m} \sum_Q \frac{\gamma_Q}{\sqrt{V}} (\boldsymbol{v}_Q \cdot \mathbf{P}(\mathbf{q}) a_Q + \text{H.c.}), \tag{4}$$

$$H_{AA} = \frac{e^2}{2m} \sum_{QQ'} \frac{\gamma_Q}{\sqrt{V}} \frac{\gamma_{Q'}}{\sqrt{V}} (\boldsymbol{v}_Q^* \cdot \boldsymbol{v}_{Q'} \hat{\rho}(\mathbf{q}' - \mathbf{q}) a_Q^\dagger a_{Q'} + \boldsymbol{v}_Q^* \cdot \boldsymbol{v}_{Q'}^* \hat{\rho}(-\mathbf{q}' - \mathbf{q}) a_Q^\dagger a_{Q'}^\dagger + \text{H.c.}). \tag{5}$$

In the last equations, $\mathbf{P}(\mathbf{q}) \equiv \int d\mathbf{x} \Psi^\dagger(\mathbf{x}) e^{i\mathbf{q}\mathbf{x}} \mathbf{p} \Psi(\mathbf{x})$ and $\hat{\rho}(\mathbf{q}) \equiv \int d\mathbf{x} \Psi^\dagger(\mathbf{x}) e^{i\mathbf{q}\mathbf{x}} \Psi(\mathbf{x})$ are, respectively, the momentum and density operators at in-plane wave vectors $\mathbf{q}$ and $\boldsymbol{v}_Q \equiv \boldsymbol{v}_Q(z = L/2)$.

The coupling constants that define the interaction terms H_{AP} and H_{AA} depend on the electronic structure of the material through the matrix elements of the momentum and density operators and on the cavity geometry through the mode functions $\boldsymbol{v}_Q$ and the amplitudes γ_Q. We keep the electronic structure fixed so that the light-matter interaction is controlled by the distance between the mirrors L.

As L is increased, the photon spectrum becomes denser, as shown in Fig. 1. Here, in order to properly take into account the effects of the light-matter interaction in both limits of small and large cavities, we retain the full multimode structure of the photon field. We notice that, in principle, the multimode QED Hamiltonian, Eq. (2), describes interaction with photon modes at all energy scales. However, as we are interested in interaction effects due to coupling with low-energy photons confined by the mirrors, we cutoff the photon spectrum at an energy Ω_{ph}. Physically, this cutoff corresponds to the largest energy of photon modes that can be confined by the cavity and is expected to be of the order of the plasma frequency of the mirrors. We assume all the effects of renormalization of the electronic properties due to interaction with photons of energy higher than the cutoff to be already included in the electronic structure defined by the periodic potential $V_{\text{periodic}}(\mathbf{x})$. If not explicitly stated otherwise the photon spectrum cutoff is set to $\Omega_{\text{ph}} = 20$ eV.

In order to ensure invariance of the results with respect to equivalent representations of the light-matter Hamiltonian, we expand the electronic Hamiltonian onto a large subspace of electronic degrees of freedom [34–39]. Specifically, we retain a total of $N_b = 30$ electronic bands.

All the presented results are converged with respect to the cutoff in the number of electronic bands. Convergence with respect to the photon cutoff will be discussed in the rest of the paper.

III. LINEAR RESPONSE THEORY

We investigate the effects of the light-matter interaction on the material properties by focusing on the long wavelength response to an arbitrary small electric field. The electronic response is defined by the conductivity tensor

$$\sigma_{ij}(\omega) = \frac{\chi_{ij}(\omega)}{i\omega} + \frac{\delta_{ij}}{i\omega}\frac{e^2}{m}\rho_0, \tag{6}$$

where ρ_0 is the average electronic density and

$$\chi_{ij}(t) = -i\theta(t)\langle\{J_i(t), J_j\}\rangle \tag{7}$$

is the current-current response function being $\mathbf{J} = \frac{1}{S}\int d\mathbf{x}\boldsymbol{j}(\mathbf{x})$ the average current density. Here we consider a system with time reversal symmetry so that $\sigma_{ij} = \delta_{ij}\sigma_{ii}$. Moreover, due to the symmetry of the square lattice $\sigma_{xx} = \sigma_{yy} = \sigma$.

Since the electronic problem is strictly two-dimensional $\boldsymbol{j}(\mathbf{x})$ represents a surface current density and is defined by the continuity equation $ie[\Psi^\dagger\Psi, H] = -\nabla\boldsymbol{j}$. The current density operator contains a purely electronic term plus a diamagnetic

contribution coming from the vacuum electromagnetic field $\boldsymbol{j}(\mathbf{x}) = \boldsymbol{j}_P(\mathbf{x}) + \boldsymbol{j}_A(\mathbf{x})$

$$\boldsymbol{j}_P(\mathbf{x}) = \frac{e}{2m}\Psi^\dagger(\mathbf{x})\mathbf{p}\Psi(\mathbf{x}) + \text{H.c.}, \tag{8}$$

$$\boldsymbol{j}_A(\mathbf{x}) = \frac{e^2}{m}\Psi^\dagger(\mathbf{x})\Psi(\mathbf{x})\mathbf{A}(\mathbf{x}). \tag{9}$$

The response function decomposes in three terms $\chi_{JJ} = \chi_{PP} + \chi_{PA} + \chi_{AA}$ defined, respectively, as the purely electronic $\chi_{PP} = \chi_{J_P,J_P}$, the mixed $\chi_{PA} = \chi_{J_P,J_A} + \chi_{J_A,J_P}$ and the purely diamagnetic $\chi_{AA} = \chi_{J_A,J_A}$ response functions. In the last definitions $J_\lambda = \frac{1}{S}\int d\mathbf{x}\ \boldsymbol{j}_\lambda(\mathbf{x})$, with $\lambda = (A, P)$, and $\chi_{J_\lambda,J_{\lambda'}}(t) = -i\theta(t)\langle[J_\lambda(t), J_{\lambda'}]\rangle$. The pure diamagnetic response χ_{AA} should not be confused with the term $\frac{e^2}{m}\rho_0$ in Eq. (6) which instead is the diamagnetic contribution of the probing field that cancels the $1/\omega$ divergence in the imaginary part of σ.

In order to compute correlation functions we make the approximation of decoupling electronic and photonic contribution in the diamagnetic term on the Hamiltonian (5) as

$$\Psi^\dagger(\mathbf{x})\Psi(\mathbf{x})\mathbf{A}^2(\mathbf{x}) \simeq \langle\Psi^\dagger(\mathbf{x})\Psi(\mathbf{x})\rangle_0\mathbf{A}^2(\mathbf{x}) + \langle\mathbf{A}^2(\mathbf{x})\rangle_0\Psi^\dagger(\mathbf{x})\Psi(\mathbf{x}), \tag{10}$$

where $\langle\cdot\rangle_0$ indicates averages computed using the noninteracting Hamiltonians. This decoupling is customarily understood in the standard definitions of Dicke-Hopfield models for QED. In particular, the $\mathbf{A}^2$ term in the Hopfield Hamiltonian is obtained by approximating the density operator with a number, which is equivalent to the decoupling in Eq. (10). As such, this approximation fully retains the effect of the $\mathbf{A}^2$ term of bounding from below the photon spectrum [40–44].

A. Current-current response functions

With the above decoupling the interaction term is such that the photonic degrees of freedom can be integrated out to obtain effective electron-electron interactions mediated by photons, see Appendix A. This fact can be conveniently used to express all the above correlation functions in term of the single-particle photon propagator, whose retarded component is defined by

$$\mathcal{D}^{\mathbf{q}'q_z'\sigma'}_{\mathbf{q}q_z\sigma}(t) = -i\theta(t)\left\langle\left[\Phi_{\mathbf{q}q_z\sigma}(t), \Phi^\dagger_{\mathbf{q}'q_z'\sigma'}\right]\right\rangle,$$

$$\Phi_{\mathbf{q}q_z\sigma} = \begin{pmatrix} a_{\mathbf{q}q_z\sigma} \\ a^\dagger_{-\mathbf{q}q_z\sigma} \end{pmatrix}. \tag{11}$$

In the empty cavity setup, the photon field has full in-plane translational invariance, i.e., $\mathcal{D} \sim \delta_{\mathbf{q}\mathbf{q}'}$. In the presence of the two-dimensional material, this is reduced to the discrete symmetry of the crystal, namely $\mathcal{D} \sim \delta_{\mathbf{q},\mathbf{q}+\mathbf{G}}$ with $\mathbf{G}$ any vector in the reciprocal lattice. However, photons of such small wavelengths correspond to energies $\hbar c|\mathbf{G}| \sim 10^3$ eV way larger than any reasonable physical energy cutoff Ω_{ph} determined by the cavity mirrors. We therefore restrict ourself to the $\mathbf{G} = 0$ case and consider, for each wave vector $\mathbf{q}$, $\mathcal{D}(\mathbf{q})$ as a matrix of dimension $2N_\mathbf{q} \times 2N_\mathbf{q}$, with $N_\mathbf{q} = 2N_z$ the number of modes with in-plane momentum $\mathbf{q}$ and energy smaller than the cutoff, where the factor 2 counts the polarizations and the 2×2 structure of the each block stems for the Nambu representation.

Thanks to Eq. (10), we incorporate the $\mathbf{A}^2$ term in the definition of the bare photon propagator $\mathcal{D}_0^{-1}(\mathbf{q},\omega) = D_0^{-1}(\mathbf{q},\omega) - \Pi_{AA}(\mathbf{q},\omega)$, being $D_0^{-1}(\mathbf{q},\omega) = \delta_{q_zq_z'}\delta_{\sigma\sigma'}(\omega\hat{\tau}_3 - \omega_{\mathbf{q}q_z\sigma} + i\Gamma_{\text{ph}}\hat{\tau}_3)$ with Γ_{ph} a small imaginary broadening mimicking dissipation through the mirrors, and $\hat{\tau}_3$ the diagonal Pauli matrix. $\Pi_{AA}(\mathbf{q},\omega)$ is the self-energy expression due to the first term in Eq. (10) and reads

$$[\Pi_{AA}(\mathbf{q},\omega)]^{(q_z'\sigma')}_{(q_z\sigma)} = \delta_{\sigma\sigma'}\frac{e^2}{m}\frac{\gamma_{\mathbf{q}q_z}}{\sqrt{L}}\frac{\gamma_{\mathbf{q}q_z'}}{\sqrt{L}}\boldsymbol{v}^*_{\mathbf{q}q_z\sigma}\cdot\boldsymbol{v}_{\mathbf{q}q_z'\sigma}\rho_0\, I\, I^\dagger. \tag{12}$$

In the last expression, I is the column vector $I = \binom{1}{1}$, so that Eq. (12) represents a 2×2 matrix in the Nambu space.

Exploiting functional integral identities, see Appendix A, the correlation functions χ_{PP} can be related to the *dressed* photon propagator $\mathcal{D}$ through

$$\left[\mathcal{D}_0^{-1}(\mathbf{q},\omega)\mathcal{D}(\mathbf{q},\omega)\mathcal{D}_0^{-1}(\mathbf{q},\omega)\right]^{(q_z',\sigma)}_{(q_z,\sigma)} - \left[\mathcal{D}_0^{-1}(\mathbf{q},\omega)\right]^{(q_z',\sigma)}_{(q_z,\sigma)} = I\, I^\dagger\ \frac{\gamma_{\mathbf{q}q_z}}{\sqrt{L}}\frac{\gamma_{\mathbf{q}q_z'}}{\sqrt{L}}\boldsymbol{v}^*_{\mathbf{q}q_z\sigma}\cdot\boldsymbol{v}_{\mathbf{q}q_z'\sigma}\chi_{PP}(\mathbf{q},\omega), \tag{13}$$

which is valid for any pair of modes (q_z,σ) and (q_z',σ). The correlation function χ_{PP} is obtained by inverting Eq. (13) for any pair of nonorthogonal modes.

The mixed correlation functions are obtained using equations of motion technique, after applying the decoupling (10) to the diamagnetic current $\boldsymbol{j}_A = \frac{e^2}{m}\rho_0(\mathbf{x})\mathbf{A}(\mathbf{x})$, being $\langle\mathbf{A}\rangle_0 = 0$. The correlation function χ_{AP} reads

$$\chi_{AP}(\mathbf{q},\omega) = \sum_{q_zq_z'\sigma}\rho_0\frac{\gamma_{\mathbf{q}q_z}}{\sqrt{L}}\frac{\gamma_{\mathbf{q}q_z'}}{\sqrt{L}}\boldsymbol{v}_{\mathbf{q}q_z\sigma}\cdot\boldsymbol{v}^*_{\mathbf{q}q_z'\sigma} \times I^\dagger[\mathcal{D}_0(\mathbf{q},\omega)]^{(q_z'\sigma)}_{(q_z\sigma)}I\ \chi_{PP}(\mathbf{q},\omega), \tag{14}$$

and χ_{PA} is obtained by computing the advanced component of (14), $\chi_{PA}(\mathbf{q},\omega) = [\chi^{adv}_{AP}(\mathbf{q},\omega)]^*$. Eventually, the purely diamagnetic contribution reads

$$\chi_{AA}(\mathbf{q},\omega) = \sum_{q_zq_z'\sigma}\rho_0^2\frac{\gamma_{\mathbf{q}q_z\sigma}}{\sqrt{L}}\frac{\gamma_{\mathbf{q}q_z'\sigma}}{\sqrt{L}}\boldsymbol{v}_{\mathbf{q}q_z\sigma}\cdot\boldsymbol{v}^*_{\mathbf{q}q_z'\sigma}I^\dagger[\mathcal{D}(\mathbf{q},\omega)]^{(q_z'\sigma)}_{(q_z\sigma)}I. \tag{15}$$

B. Photon propagator

Equations (13)–(15) reduce the problem of the computation of the response function to the computation of the dressed photon propagator $\mathcal{D}$. We compute the photon propagator by treating the electron-photon interaction at the level of Gaussian fluctuations. This approach corresponds to dressing the photon propagator with the bare current-current response function. The Dyson equation for the matrix $\mathcal{D}(\mathbf{q},\omega)$ reads

$$\mathcal{D}^{-1}(\mathbf{q},\omega) = \mathcal{D}_0^{-1}(\mathbf{q},\omega) - \Pi_0(\mathbf{q},\omega) \tag{16}$$

with the block components of the self-energies

$$[\Pi_0(\mathbf{q},\omega)]^{(q_z'\sigma)}_{(q_z\sigma)} = \frac{\gamma_q}{\sqrt{V}}\frac{\gamma_{q'}}{\sqrt{V}}\boldsymbol{v}_{\mathbf{q}q_z\sigma}\cdot\boldsymbol{v}_{\mathbf{q}q_z'\sigma}\chi^0(\mathbf{q},\omega)II^\dagger. \tag{17}$$

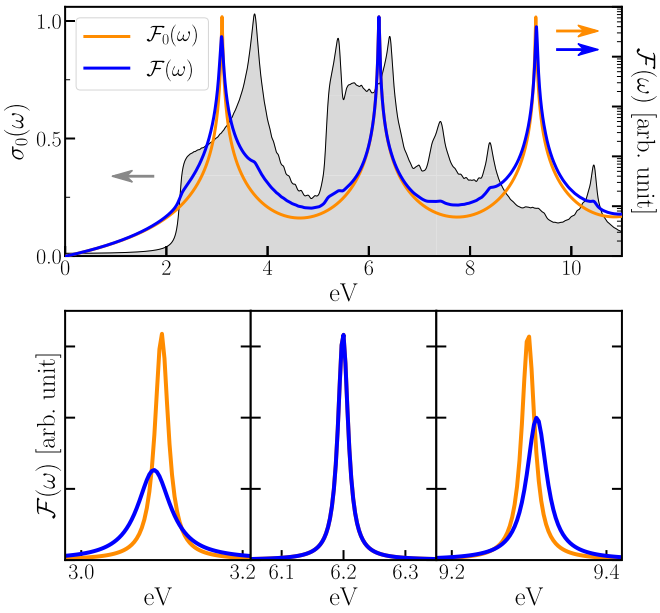

FIG. 2. Bare $\mathcal{F}_0(\omega)$ and dressed $\mathcal{F}(\omega)$ spectral densities for the $\mathbf{q}=0$ photons for cavity mirrors at a distance $L=0.2$ μm. Bare photons broadening is set to $\Gamma_{\rm ph}=0.01$ eV. Shaded area represents the bare conductivity of the material. Throughout the paper the conductivity is measured with respect to the quantum of conductance $G_0\equiv\frac{2e^2}{h}$. The conductivity is plotted in the linear scale, while photon spectra are plotted in the logarithmic scale (see arrows). Bottom panels show the photon spectral densities in linear scale around the single photon resonances.

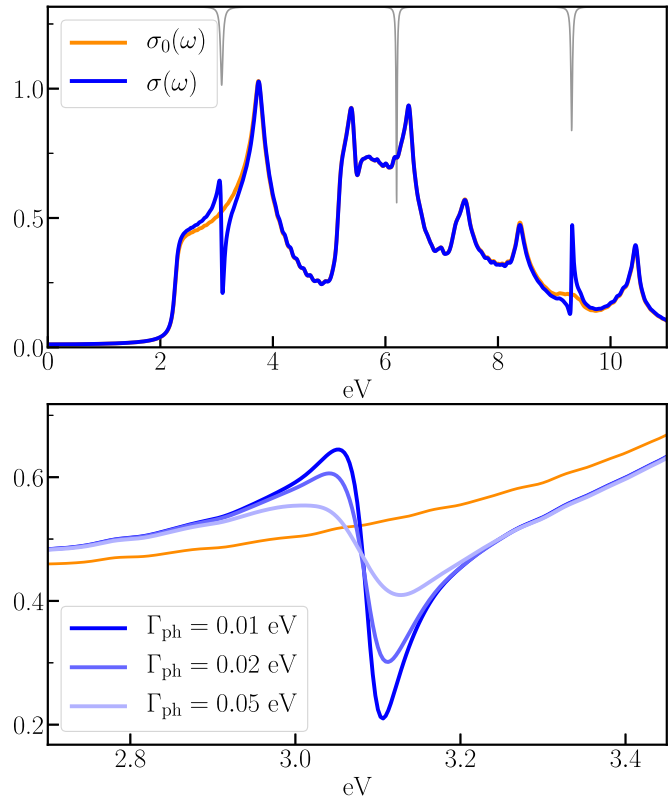

FIG. 3. (Top) Bare σ_0 (orange) and dressed σ (blue) conductivities for cavity length $L=0.2$ μm. The inverted photon spectrum is reported in the top part of the panel. Photon broadening is $\Gamma_{\rm ph}=0.01$ eV. (Bottom) Blow up of the asymmetric feature in the dressed conductivity around 3.1 eV for different values of the photon broadening.

$\chi^0(\mathbf{q},\omega)$ is the current-current response function for the electronic system computed in the absence of the light-matter interaction

$$\chi^0(\mathbf{q},t)=-i\theta(t)\langle[\mathbf{J}^0_{-\mathbf{q}}(t),\mathbf{J}^0_{\mathbf{q}}]\rangle_0 \tag{18}$$

with

$$\mathbf{J}^0_{\mathbf{q}}=\frac{e}{m}\mathbf{P}(\mathbf{q})=\frac{e}{m}\sum_{\mathbf{k}\nu\nu'}\mathbf{p}^{\mathbf{k}\nu'}_{\mathbf{k}+\mathbf{q}\nu}c^\dagger_{\mathbf{k}+\mathbf{q}\nu}c_{\mathbf{k}\nu'} \tag{19}$$

with $\mathbf{p}^{\mathbf{k}\nu'}_{\mathbf{k}+\mathbf{q}\nu}=-i\hbar\int d\mathbf{x}\varphi^*_{\mathbf{k}+\mathbf{q},\nu}e^{i\mathbf{q}\mathbf{x}}\nabla\varphi_{\mathbf{k}\nu'}(\mathbf{x})$, being $\varphi_{\mathbf{k}\nu}(\mathbf{x})$ the Bloch functions. Computation of the bare response function reduces to simple convolutions of single-particle Greens functions. In Matsubara frequencies, this reads

$$\chi^0(\mathbf{q},i\Omega_n)=\frac{e^2}{m^2}\sum_{\mathbf{k}\nu\nu'}\left|\mathbf{p}^{\mathbf{k}\nu'}_{\mathbf{k}+\mathbf{q}\nu}\right|^2 \times T\sum_{i\omega_n}G^0_{\mathbf{k}+\mathbf{q},\nu}(i\omega_n+i\Omega_n)G^0_{\mathbf{k},\nu'}(i\omega_n) \tag{20}$$

with $G^0_{\mathbf{k}}(i\omega_n)=(i\omega_n-\epsilon_{\mathbf{k}\nu})^{-1}$ with $i\Omega_n$ and $i\omega_n$ representing, respectively, bosonic and fermionic Matsubara frequencies. The retarded component is therefore obtained through analytical continuation $i\Omega_n\to\Omega+i0^+$. Eventually, χ^0 is plugged into Eq. (17) to get the dressed photon propagator.

IV. OPTICAL DRESSING OF THE ELECTRONIC RESPONSE

In this section, we present the main results showing the effects of the light-matter hybridization in the homogeneous ($\mathbf{q}=0$) response obtained using the above approximation scheme. As it is clear from Eqs. (13)–(15), in the Gaussian approximation only the $\mathbf{q}=0$ photons contribute to the dressing of the $\mathbf{q}=0$ response. Corrections beyond the Gaussian approximation will include interaction with photons at finite in-plane momentum and will be discussed in Sec. V B.

In Fig. 2, we report the total spectral density of photons at zero in-plane momentum $\mathcal{F}_\sigma(\omega)=-\frac{1}{\pi}\sum_{q_z,q_z'}\mathrm{Im}[\mathcal{D}^{11}(\mathbf{q}=0,\omega)]^{(q_z'\sigma)}_{(q_z\sigma)}$ for a cavity with $L=0.2$ μm. The symbol $\mathcal{D}^{11}$ denotes the normal component, i.e., $\langle aa^\dagger\rangle$, of the Nambu photon propagator. Due to the symmetry of the problem the spectral density is polarization independent $\mathcal{F}_\sigma(\omega)=\mathcal{F}(\omega)$. The bare and interacting spectral densities are superimposed to the bare optical conductivity of the system which characterizes the absorption of the material in the absence of hybridization with vacuum photons. The dressed photon spectral density is characterized by a shift of the resonances and by a broad redistribution of spectral weight indicating hybridization with the continuum of optical excitations in the material. Due to the symmetry of the mode functions the dressing vanishes in correspondence to the even, i.e., $n=2m$, modes for which $\boldsymbol{v}(z=L/2)=0$.

The broad photon dressing corresponds to sharp features in the conductivity. In Fig. 3, we report the dressed conductivity $\sigma(\omega)$, computed through Eqs. (6) and (13)–(15). By

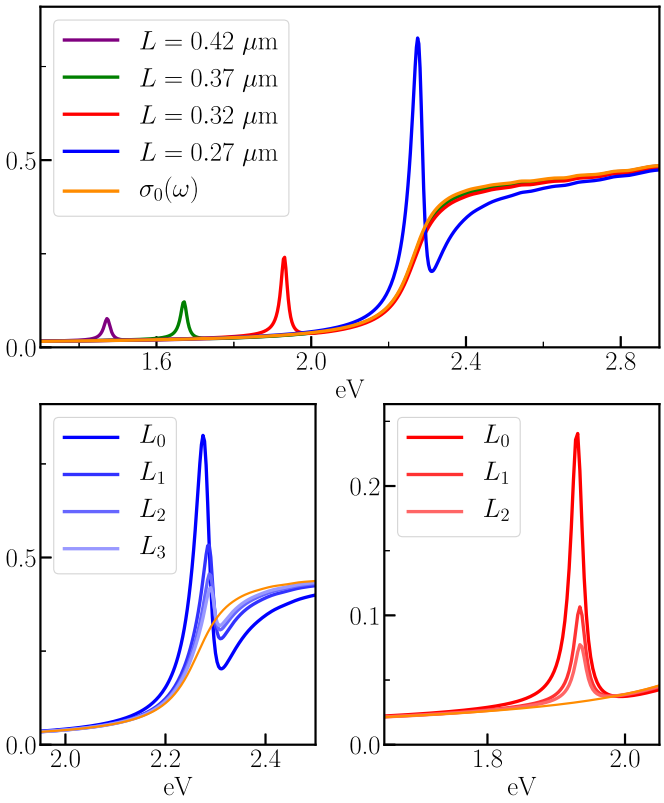

FIG. 4. (Top) Dressed conductivity at different cavity lengths. (Bottom) Conductivity at resonant lengths $L_n = (2n+1)L_0$ for $L_0 = 0.27$ (left) and $0.32\ \mu$m (right).

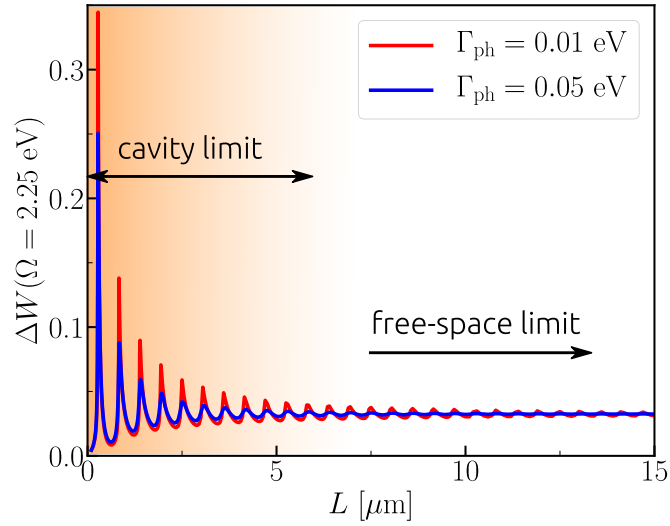

FIG. 5. Spectral weight transfer below the gap edge $\Omega_{\rm gap} = 2.25$ eV as a function of the distance between the mirrors for two values of the photon damping. The shaded area highlights the crossover from the cavity to the free-space limit.

comparing to the bare conductivity $\sigma_0(\omega)$ we observe sharp asymmetric shifts of spectral weight in correspondence of the dressed photon modes. This asymmetric shift is reminiscent of a Fano-like profile clearly highlighting the hybridization of a single photon mode with the continuum of electronic excitations. The amount of redistributed spectral weight depends on the broadening of the photon modes $\Gamma_{\rm ph}$, decreasing for larger damping.

The resonant frequency of the asymmetric shift is modified by acting on the cavity length. Figure 4 reports the cases in which the resonances appear, respectively, at the gap edge and inside the optical gap. In the former case, we show a modification of the optical gap characterized by the formation of a sharp peak at the gap edge with sizable absorption below the bare gap. When the resonance moves inside the gap, we instead observe the formation of in-gap absorption peaks. In-gap peaks are much weaker with respect to the sharp resonances appearing above gap. This is understood as, due to the vanishing small optical absorption, light-matter hybridization below gap is progressively suppressed. Experimental investigations along these lines have been carried out in the context of semiconductor microcavities embedding intersubband transitions [12] following the theory in Ref. [45].

We investigate the effects of confinement on the dressing by looking at cavity lengths $L_n(\Omega_0)$ featuring a resonant mode at frequency Ω_0. The resonance condition is set by

$$L_n = (2n+1)L_0 \tag{21}$$

being $L_0 = \hbar c \frac{\pi}{\Omega_0}$ the length of a cavity with fundamental mode at the frequency Ω_0. The integer $l = 2n+1 = \frac{2L}{\lambda}$ counts the number of half-wavelengths contained in the cavity. As shown in the bottom panels of Fig. 4, the dressing is suppressed as n is increased. This fact can be directly correlated to the strength of the coupling constants in the Hamiltonian which, for a mode at fixed frequency Ω_0, scales as $\gamma_Q/\sqrt{L} \sim 1/\sqrt{\Omega_0 L} \sim 1/\sqrt{l}$.

We summarize the effect of light-dressing on the conductivity by considering the relative amount of spectral weight which is transferred below the gap. We define the relative variation of spectral weight below a given frequency Ω as

$$\Delta W(\Omega) \equiv \frac{\int_0^\Omega d\omega[\sigma(\omega) - \sigma_0(\omega)]}{\int_0^\Omega d\omega \sigma_0(\omega)}. \tag{22}$$

As expected from conductivity sum rules, our results correctly predict conservation of total spectral weight $\lim_{\Omega\to\infty} \Delta W(\Omega) \to 0$. Figure 5 show the evolution of $\Delta W(\Omega = \Omega_{\rm gap})$ computed at the energy of the bare direct optical gap $\Omega_{\rm gap} = 2.25$ eV, as a function of the distance between the mirrors. The resonant transfer of spectral weight below the gap is reflected in the oscillating behavior of ΔW. Maxima of transferred spectral weight correspond to cavity modes resonant with the band edge. The intensity of the maxima decreases with L, as anticipated by the results in Fig. 4. Eventually for $L \gtrsim 5\ \mu$m, the amplitude of oscillations gets significantly suppressed and the transferred spectral weight smoothly evolves towards an asymptotic value independent of L. This evolution clearly highlights the crossover from a regime in which the effects of the cavity confinement are predominant to the free-space regime in which mirrors becomes irrelevant.

Remarkably, we find that a residual finite dressing, corresponding to few percent shift of the spectral weight, persists up to the free space limit. The dressing in the free-space limit

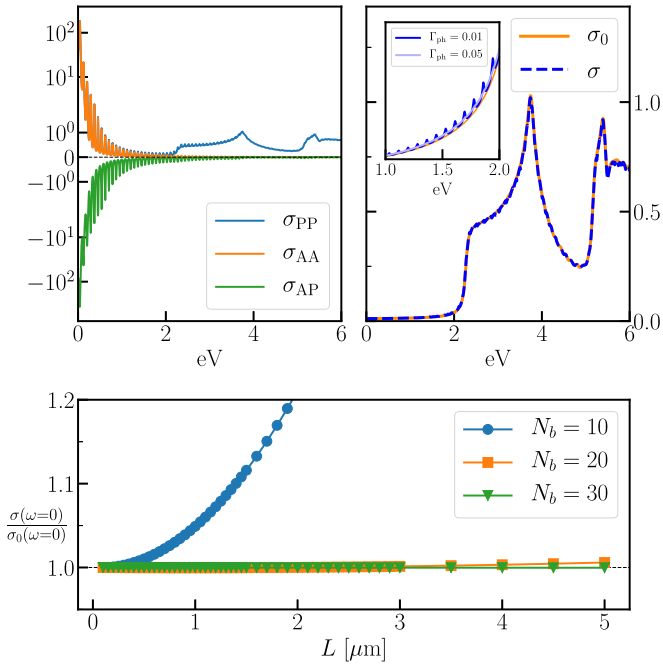

FIG. 6. (Top) Dressed conductivity in the large L limit $L = 15$ μm. (Left) Purely electronic σ_{PP}, purely diamagnetic σ_{AA} and mixed σ_{AP} contributions to the conductivity. (Right) Bare conductivity σ_0 (orange full) compared to the dressed conductivity $\sigma = \sigma_{PP} + \sigma_{AP} + \sigma_{AA}$ (blue dashed). (Inset) Zoom of the dressed conductivity below the gap showing the transferred spectral weight for two values of the photon damping $\Gamma_{\rm ph}$. (Bottom) Dressing of conductivity in the static limit as a function of the cavity length, and for different cutoff in the number of electronic bands N_b.

can be understood as the regime in which the suppression of the couplings due to the larger cavity is balanced by the increasing density of photon modes. As physically expected, the free-space dressing becomes independent of the photon broadening $\Gamma_{\rm ph}$. In contrast, in the cavity limit a larger damping corresponds to a smaller shift of the spectral weight.

The effects of the light-matter hybridization in the free-space limit can be appreciated by separately looking at the purely electronic σ_{PP}, purely diamagnetic σ_{AA} and mixed σ_{AP} contributions that defines the dressed conductivity as $\sigma(\omega) = \sigma_{PP}(\omega) + \sigma_{AP}(\omega) + \sigma_{AA}(\omega)$, see Eqs. (13)–(15), reported in Fig. 6 for $L = 15$ μm. If the couplings with all the photon modes were set to zero, the various contributions would reduce to $\sigma_{AP} = \sigma_{AA} = 0$ and $\sigma_{PP} = \sigma_0$. However, due to the finite density of modes at low energy the single contributions shows the $\sim 1/\omega$ divergence as $\omega \to 0$ and the full dressed conductivity reduces to $\sigma \simeq \sigma_0$ due to the cancellation of terms. The cancellation is perfect at $\omega \to 0$, whereas it leads to a residual shift of spectral weight at finite frequency, see inset in Fig. 6.

The perfect cancellation of the dressing of the static conductivity holds true for all values of cavity lengths, see Fig. 6 bottom panel. Specifically, we found that the cancellation can be highly sensitive to the cutoff in the number of electronic bands included in the calculation N_b. Indeed, if N_b is too small, the cancellation of terms is not perfect, and a finite dressing of the dc conductivity appears for large cavities. This dressing is fictitious and disappears as soon as the electronic cutoff is increased. The sensibility of static quantities to the truncation of the electronic spectrum is a well known feature of the representation of the light-interaction Hamiltonian adopted in this work, Eqs. (4) and (5). Convergence with respect to the truncation of the electronic subspace can be understood as a the fulfillment of optical sum rules for coupling constants [34–37].

We end this section by observing that all the results presented so far are converged with respect to the cutoff in the photon spectrum. Specifically, the cutoff was set to $\Omega_{\rm ph} = 20$ eV whereas reasonable convergence is already reached for $\Omega_{\rm ph} \gtrsim 10$ eV.

V. CLASSICAL DESCRIPTION AND QUANTUM CORRECTIONS

The above results indicate that the electronic conductivity contains a contribution from vacuum photons that is larger the smaller the confining volume provided by cavity mirrors. The effect of light-matter hybridization can be generically ascribed to photon fluctuations in vacuum. However, it is possible to give a more practical physical description of this dressing. The conductivity measures the fluctuations of the currents in response to an arbitrary small field. These current fluctuations act as sources of electromagnetic fields which, in turn, have a feedback on the current fluctuations.

This observation brings to fundamental question: to what extent can the optical dressing of the electronic response be described in terms of classical fields sourced by current fluctuations in matter? In this section we address this question by considering a classical description of the light-matter hybridization and comparing it to the quantum description including corrections beyond the Gaussian approximation presented in the previous section.

A. Classical description

The classical description of the conductivity dressing builds on the definition of a current in response to an arbitrary small applied field. Calling $J[E_0]$ the current in response to a field E_0 polarized along x we introduce the decomposition

$$J[E_0] = J_0[E_0] + \delta J[E_0]. \tag{23}$$

$J_0 = \sigma_0 E_0$ is the bare current defined by the bare conductivity σ_0, whereas δJ is the correction to the current which is due to the field E sourced by the current itself. Since E_0 is arbitrarily small we can assume that also E is small so that we can write $\delta J = \sigma_0 E$. Eventually, we can define the dressed conductivity as

$$\sigma(\omega) = \lim_{E_0 \to 0} \frac{\partial J[E_0]}{\partial E_0} = \sigma_0(\omega)(1 + \eta(\omega)) \tag{24}$$

with $\eta(\omega) = \lim_{E_0 \to 0} \frac{\partial E}{\partial E_0}$ the correction to the bare σ_0.

We compute the correction $\eta(\omega)$ by using Maxwell's equation with J defined in Eq. (23) as a source term. For the geometry considered in this work the Maxwell's equations reduce to the one-dimensional wave equation

$$\frac{\partial^2 E(z,t)}{\partial z^2} - \frac{1}{c^2}\frac{\partial^2 E(z,t)}{\partial t^2} = \mu_0 \delta(z) \frac{\partial J(t)}{\partial t} \tag{25}$$

with boundary conditions $E(\pm L/2) = 0$. We expand the field in plane waves and transform to the frequency domain. To compare with the result of the previous section we add an imaginary damping $\omega \to \omega + i\Gamma_{\rm ph}$ to match the broadening of the photon lines. Solving the wave-equation for $\frac{E(z,\omega)}{E_0}$, the correction to the conductivity is obtained as $\eta(\omega) = \frac{E(z=0,\omega)}{E_0(\omega)}$. Close to a resonance ω_0 of the cavity, this gives

$$\sigma(\omega) \simeq \sigma_0(\omega)\left[1 - \frac{i\kappa}{\omega - \omega_0 + i(\kappa + \Gamma_{\rm ph})}\right] \qquad (26)$$

with $\kappa = \mu_0\sigma_0(\omega_0)/L$. The equation (26) describes a shift of the spectral weight centered in ω_0. Specifically, the response is completely suppressed for $\omega = \omega_0$ when the damping is sent to zero $\Gamma_{\rm ph} \to 0^+$. The spectral weight is therefore moved to higher (lower) frequencies depending on the positive (negative) sign of the imaginary part of σ_0. By taking the static limit of Eq. (25), we also notice that the correction trivially vanishes for $\omega \to 0$, therefore matching the perfect cancellation of the dressing of the dc conductivity discussed at the end of Sec. IV.

In Fig. 7, we plot the dressed conductivity obtained by solving the wave equation (24) for the full multimode structure of the cavity. The dressed conductivity shows remarkable agreement with the results of previous section obtained by applying the Gaussian approximation to the QED Hamiltonian. For simplicity, we explicitly show in Fig. 7 the comparison for the dressing of conductivity only in the limit of small cavity. However, we found the same perfect agreement also for the dressing in the free-space limit.

To see how the agreement depends on the overall coupling strength we introduce a parameter Z to renormalize the charge of the electron as $e \to \sqrt{Z}e$ so that the optical absorption of the semiconductor increases linearly with Z. As shown in the bottom panel of Fig. 7, increasing Z results in a stronger dressing of the photon spectral density. Specifically, we see that $Z = 50$ produces a huge shift $\sim$0.4 eV of the energy of the fundamental mode. This corresponds to an even larger shift of spectral weight in the optical conductivity with a modification of the optical gap of about $\sim$0.5 eV, clearly indicating a regime of strong coupling between light and matter.

Even in this strong coupling regime the dressing of the optical conductivity computed using Dyson equation for the photon propagator perfectly matches the one computed by using Maxwell's equation. We therefore conclude that, independently of the strong coupling regime, the classical description fully reproduces results of Gaussian approximation for the QED Hamiltonian.

We emphasise that this strong coupling regime, signalled by a large shift of the photon resonance and spectral weight in the electronic response, is equivalent to a large polariton splitting due to the hybridization of a single photon mode with single matter excitations, such as excitons or intersubband transitions [40,46–48]. The absence of the double peak structure in the photon spectra [Fig. 7(b)] is due to the fact that in the present case photons hybridize with a continuum of electronic transitions giving rise to a smooth absorption spectrum. The results presented can be readily extended to the case in which the absorption spectrum is characterized by sharp resonances and we do not expect major changes to the underlying physics.

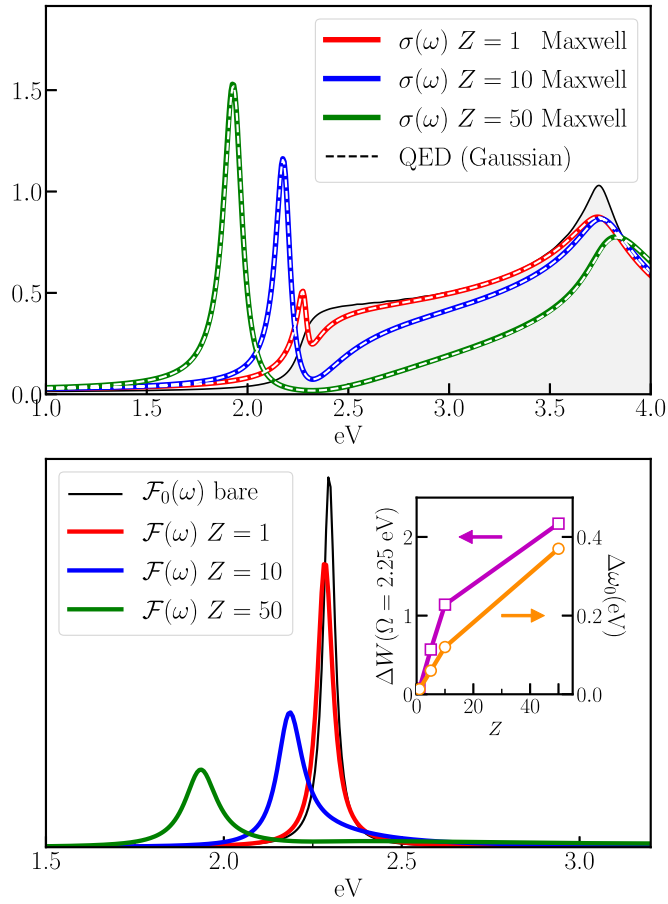

FIG. 7. (Top) Dressed conductivity computed using current dressing in Maxwell's equations (full lines) for different values of the charge renormalization parameter $Z = 1$ (red), 10 (blue), and 50 (green). White dashed lines indicate the same quantities computed from the QED Hamiltonian in the Gaussian approximation for the same values of Z. For comparison, the conductivity curves have been scaled by the factor Z. The cavity length is $L = 0.27$ μm and the broadening $\Gamma_{\rm ph} = 0.02$ eV. Bottom: Photon spectral densities around the cavity fundamental mode computed using the QED Hamiltonian in the Gaussian approximation for the same values of Z shown above. Insets: shift of the photon resonance of the fundamental cavity mode as a function of Z (circles, right axis). $\Delta\omega_0$ is defined as the energy difference between the peak of the bare $\mathcal{F}_0$ and the peak of the dressed $\mathcal{F}$. Relative shift of the spectral weight Eq. (22) as a function of Z (squares, left axis).

B. Quantum corrections

The perfect agreement between the classical regime and Gaussian treatment of the QED Hamiltonian can be expected as only the bare response function χ_0 enters in the dressing of the photon propagator at the Gaussian level in the same way as only the bare conductivity σ_0 enters in the classical correction Eq. (24). Therefore corrections to the classical results must be encoded in the corrections beyond the Gaussian approximation for the photon propagator.

In this section, we estimate the size of such quantum corrections by focusing on the lowest order electronic self-energy corresponding to the dressing of the electron propagator with a single photon line (see sketch in Fig. 8). The self-energy

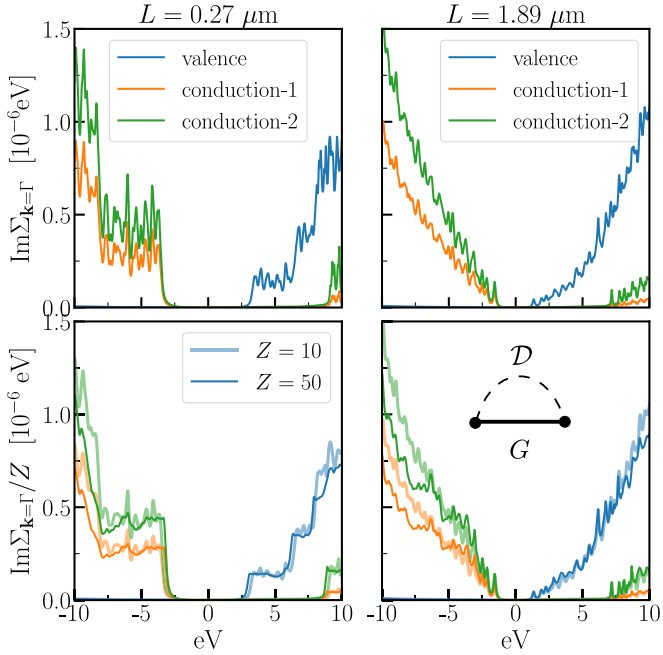

FIG. 8. Imaginary parts of the electronic self-energy computed at the Γ point for the valence and first two conduction bands and for two cavity lengths $L = 0.27$ (left) and 1.89 μm (right). Top panels show the self-energies for $Z = 1$. Bottom panels show self-energies divided by Z for $Z = 10$ and 50. In the bottom right panel we reported a sketch of the self-energy diagram considered. The full line indicates the electronic Green's function G, while the dashed line indicates the photon propagator $\mathcal{D}$. The dots indicate the couplings. For simplicity, in the sketch we omitted all the labels of quantum numbers as well as the energy and momentum conservation at the vertices. The noise in the self-energies is due to the discretization of the $\mathbf{q}$ grid for momentum integration of the photon propagator.

expression reads

$$[\Sigma(\mathbf{k}, i\omega_n)]_{(\nu,\nu')} = \frac{1}{S}\sum_{\mathbf{q}}\sum_{\substack{q_z\sigma\\ q_z'\sigma'}}\sum_{\mu\mu'} T\sum_{i\Omega_n} KI^{\dagger}[\mathcal{D}(\mathbf{q}, i\Omega_n)]^{(q_z'\sigma')}_{(q_z\sigma)} I \times [G(\mathbf{k}+\mathbf{q}, i\omega_n + i\Omega_n)]_{\mu\mu'}. \quad (27)$$

The constant K depends on all the outer and inner indices and is defined as $K \equiv \frac{\gamma_{\mathbf{q}q_z}}{\sqrt{L}}\frac{\gamma_{\mathbf{q}q_z'}}{\sqrt{L}}(\boldsymbol{v}_{\mathbf{q}q_z\sigma}\cdot\mathbf{p}^{\mathbf{k}\mu}_{\mathbf{k}+\mathbf{q}\nu})(\boldsymbol{v}_{\mathbf{q}q_z'\sigma'}\cdot\mathbf{p}^{\mathbf{k}\mu'}_{\mathbf{k}+\mathbf{q}\nu'})^*$. The self-energy corrections are used to dress the single-particle electronic Greens function G, which enters in the definition of the self-energy for the photon propagator. Eventually, a self-consistent procedure is established to simultaneously obtain the dressed electronic and photon propagators [27].

Before computing the self-energy we estimate the order of magnitude of the corrections by considering a single electronic transition $\nu \to \mu$ and replacing the photonic and electronic propagators in Eq. (27) with the bare ones. The integration over in-plane momenta $\frac{1}{S}\sum_{\mathbf{q}} \to \int \frac{d\mathbf{q}}{(2\pi)^2}$ is restricted at momenta $|\mathbf{q}| < q_c = \frac{\Omega_{\mathrm{ph}}}{\hbar c}$. For cutoff energies $\Omega_{\mathrm{ph}} \sim 10$–$20$ eV the momentum cutoff is $q_c \ll \frac{\pi}{a}$ so that the integration domain corresponds to a small region around the $\mathbf{q} = 0$ point in the Brillouin zone. This fact allows to take the fermionic propagator out of the integral $G_0(\mathbf{k}+\mathbf{q}) \simeq G_0(\mathbf{k})$. We define the constant $K_{\nu\mu}(\mathbf{k}) = \frac{\hbar^2 e^2}{2\epsilon_0 m^2}|\mathbf{p}^{\mathbf{k}\mu}_{\mathbf{k}\nu}|^2$ and take the summation over the frequencies. We obtain, after analytical continuation, $\mathrm{Im}\Sigma_{\nu\to\mu}(\mathbf{k},\omega) \sim K_{\nu\mu}(\mathbf{k})[b(\epsilon_{\mathbf{k}\mu}-\omega) + f(\epsilon_{\mathbf{k}\mu})]\Delta(\epsilon_{\mathbf{k}\mu}-\omega)$, with b and f the Bose and Fermi functions, respectively. The function $\Delta(\Omega)$ is defined by the photon density of states $\rho_{\mathrm{ph}}(\Omega)$ as $\Delta(\Omega) = \frac{\rho_{\mathrm{ph}}(\Omega)-\rho_{\mathrm{ph}}(-\Omega)}{|\Omega|}$ with $\rho_{\mathrm{ph}}(\Omega) \simeq \frac{\theta(\Omega)}{\pi^2}\frac{\Omega^2}{(\hbar c)^3}$. In the last approximation, we considered the density of states in the continuum limit. At low temperatures, the phase space for the electron-photon scattering is $b(\epsilon_{\mathbf{k}\mu}-\omega) + f(\epsilon_{\mathbf{k}\mu}) \sim -\mathrm{sgn}(\omega)\theta(|\omega| - |\epsilon_{\mathbf{k}\mu}|)$. The largest contributions in the function Δ come from the smallest values of $|\epsilon_{\mathbf{k}\mu}|$, so that we estimate the order of magnitude of the self-energy by taking $\Delta(\epsilon_{\mathbf{k}\mu}-\omega) \sim \Delta(-\omega)$ from which $\mathrm{Im}\Sigma_{\nu\to\mu}(\mathbf{k},\omega) \sim K_{\nu\mu}(\mathbf{k})\frac{\rho_{\mathrm{ph}}(|\omega|)}{|\omega|}$. By assuming $|\mathbf{p}^{\mu}_{\nu}| \sim \frac{\pi}{a}$, the constant is $K_{\nu\mu}(\mathbf{k}) \sim Z \times \mathrm{eV}^3\,\mathrm{nm}^3$ being Z the electronic charge renormalization constant. On the other hand the photon density of states is $\rho(|\omega|)/|\omega| \sim |\omega| \times 10^{-7}\ \mathrm{eV}^{-3}\,\mathrm{nm}^{-3}$. We therefore obtain $\mathrm{Im}\Sigma_{\nu\mu} \sim Z|\omega|\theta(|\omega| - \omega_0) \times 10^{-7}$ eV being ω_0 the fundamental mode of the cavity.

The above estimation, valid for a single electronic transition, is confirmed by numerically integrating the self-energy using the dressed photon propagator and including all the electronic transitions within the cutoff in the number of electronic bands. Figure 8 reports the imaginary part of the self-energy computed at the Γ point for the valence and the first two conduction bands. We consider two values of cavity lengths characterized by modes resonant with the gap edge for which the largest modification of the optical gap is observed, see Fig. 4. The self-energies are characterized by some noise which is due to the finite grid used to discretize the $\mathbf{q}$ space for momentum integration of the photon propagator.

$\mathrm{Im}\Sigma$ vanishes for frequencies smaller than the fundamental mode of the cavity and than increases with $|\omega|$ remaining of the order of $\lesssim 10^{-6}$ eV for $|\omega| \lesssim 10$ eV, in agreement with the above estimation obtained for a single electronic transition. In the limit of small cavity it is possible to appreciate a step-like behavior due to characteristic jumps in the photon density of states. The jumps are washed out for larger cavities due to the smoother density of state of photons. We also show that the self-energy scales linearly with Z (bottom panels). For larger Z, the self-energies are less noisy due to the additional broadening in the photon spectral density due to the strong coupling dressing.

Figure 9 reports the real part of the self-energy which measures the renormalization of the energies of the single-electron excitation as given by the pole equation $\omega_* - \varepsilon_{\mathbf{k}\nu} - \mathrm{Re}\Sigma_{\nu\nu}(\mathbf{k},\omega_*) = 0$. We observe that the real-part has an intrinsic dependence on the photon cutoff Ω_{ph}. This dependence is readily understood as the real part is related to the imaginary part via a Kramers-Kronig transformation (KKT) $\mathrm{Re}\Sigma(\omega) = -\frac{1}{\pi}\int d\omega' \frac{\mathrm{Im}\Sigma(\omega')}{\omega-\omega'}$. Since the imaginary part is proportional to the photon density of states it increases as a function of frequency up to the cutoff Ω_{ph} after which it drops to zero. Therefore a larger high-energy cutoff will result in a larger real part at low frequencies.

This observation indicates that renormalization of the electronic poles by self-energy corrections are actually dominated by off resonant high-energy modes. As the photon density of states diverges at $\omega \to \infty$, we would expect a divergent real-part for $\Omega_{\mathrm{ph}} \to \infty$. We expect this divergence to correspond to

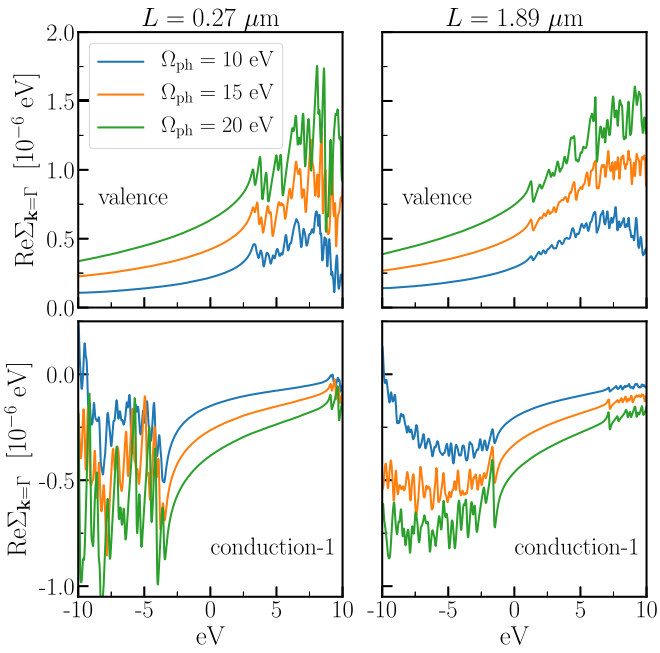

FIG. 9. Real parts of the electronic self-energy computed at the Γ point for the valence (top) and first conduction (bottom) bands and for two cavity lengths $L = 0.27$ (left) and $1.89\ \mu$m (right). Panels show self-energies for $Z = 1$ and different cutoff energies $\Omega_{ph} = 10$ eV, $\Omega_{ph} = 15$ eV, and $\Omega_{ph} = 20$ eV.

the well known divergences encountered in the nonrelativistic description of effects like Lamb shifts. These divergences are generically cured by introducing a cutoff at the order of the Compton scale [49]. As the goal here is to understand the effects of the photons confined by the mirrors below the physical cutoff of the plasma frequency, we have assumed that all the effects of photons at such high-energy scales to be already included in the definition of the bare electronic dispersion, see Sec. II C. As such, we can argue away these divergences and restrict ourselves to the interaction effects below the physical cutoff Ω_{ph} and focus on their dependence on the cavity confinement.

For cutoff in the $\Omega_{ph} \sim 10$–20 eV range the real part of the self-energy remains of the same order of magnitude of the imaginary one. Even considering a very large $Z \sim 10^2$ corrections in the eV range are of the order $\lesssim 10^{-4}$ eV, meaning that, compared to typical electronic energy scales, renormalization of the pole of the electronic Green's function can be considered as negligible. Most importantly, we observe that the overall magnitude of the corrections weakly depends on the cavity confinement which is consistent with the above arguments showing that the renormalization mostly depends on the cutoff.

We point out that the smallness of these corrections can be generically ascribed to the smallness of the photon density states at low energies. To better appreciate this aspect, it is useful to compare the density of states of photons with that of acoustic phonons which have the same dispersion of photons, with speed of sound $c_0 \ll c$, and couple to electrons in a similar way, with different matrix elements. At variance with photons, phonons have an intrinsic low-energy cutoff set by the lattice, whereas the photon spectrum is unbounded. It is immediate to see that at low-energies the phonon density of states is enhanced by the factor $(c/c_0)^d \gg 1$ being d the dimensionality of the system. It follows that, while scattering with phonons at low energy generically leads to a dressing of the electronic Green's function, in the case of photons the largest effects are expected to come from off resonant modes at high energies for which the density of states becomes large. Since the cavity modifies the photon spectrum only below the mirrors' plasma frequency, it is conceivable that cavity confinement has a small effect on the photon-dressing of the single-particle electron Green's function as shown in Figs. 8 and 9.

Based on these observations we conclude that, for all practical purposes, dressing of the electronic Green's function due to low-energy photons confined by the cavity can be neglected. We emphasise that this phenomenology is intrinsically different from the results in Sec. IV which are instead fully converged with respect to the cutoff Ω_{ph} and can be explained without invoking any modification of the single-electron excitation energies.

Calculation of higher order corrections, included the vertex corrections related to the decoupling of the diamagnetic term, Eq. (10), are beyond the scope of this work. However, we expect that similar arguments related to the small photon density of states at low-energy and to the unbound growth of density of states up to relativistic energies to apply also to higher-order corrections.

The main consequence of the above observations is that corrections to the Gaussian approximation used for the computing the photon propagator are expected to be small and, in general, weakly dependent on the confinement of the mirrors. As a result, having shown that results in the Gaussian approximation can be fully reproduced using the classical description independently of the strength of the coupling, we conclude that quantum effects due to confinement of low-frequency photons can be considered negligible.

VI. CONCLUSIONS

In this paper we have studied the modification of the electronic properties due to light-matter hybridization in a planar cavity. We have focused on the electronic conductivity of a two-dimensional material placed in between two parallel mirrors that confine the electromagnetic field on a length scale L. We have treated the light-matter interaction by considering the multimode expansion of the nonrelativistic QED Hamiltonian including all the photon modes below an energy cutoff Ω_{ph}, physically corresponding to the plasma frequency of the mirrors.

We have shown sharp signatures of the light-matter hybridization corresponding to sizable redistribution of spectral weight at resonant frequencies. At the gap edge for optical absorption, the light-matter hybridization results into a renormalization of the optical gap. Following the conductivity as a function of the distance between the mirrors, we have described the crossover from the cavity to the free-space limit. In the cavity limit, the confinement gives rise to significantly larger shifts of the spectral weight. In the free-space limit, we observe a residual dressing which is independent of the mirrors.

We have shown that both limits can be accurately reproduced using a classical description in which current fluctuations get dressed by self-interaction with the fields sourced by the current fluctuations. By introducing an effective renormalization of the electronic charge, we have demonstrated that the classical description remains valid even in the strong coupling regime, where the shift of the cavity resonance due to the light-matter interaction becomes of a sizable fraction of its bare value.

Using this comparison, we have investigated the quantum effects of the light-matter interaction by considering corrections beyond the Gaussian approximation. We have shown that for low-energy photons confined in the cavity, these corrections are negligibly small up to the very strong coupling regime. Most importantly, these corrections weakly depend on the cavity confinement. As a result, the single-particle properties are not substantially modified by the cavity confinement.

Our results indicate that, despite a significant effect of light-matter dressing on the optical gap, the strong coupling regime does not automatically correspond to an equally large modification of the single-particle properties, namely the electronic dispersion and the electronic band gap. This difference can be understood by observing that the response functions contributing to the optical conductivity have poles at the energies of the so-called bright polaritons, which correspond to the transitions from the ground state to an excited state with the same number of electron upon emission or absorption of a photon. On the contrary, the poles in the single-particle Green's functions are determined by the virtual transitions from the ground states to all excited states with one particle added or removed. Therefore, unlike the response functions, the poles in the single-particle Green's function have no direct connection with the bright or dark polaritons.

The large modifications of the electronic response are mostly captured by the classical Maxwell equations, thus reducing optical dressing due to the low-energy photons confined by the cavity to an essentially classical effect. While the modifications of the electronic response appear in agreement with recent spectroscopic experiments [12], future work is required to unravel implications of these results for different physical situations, such as, for example, the response beyond the linear regime, electroluminescence or problems of quantum transport [50–54], and magnetotransport [30,31].

We stress that our results take into account only the effects of fluctuations of the transverse photons, while we have neglected effects associated with the longitudinal part of the electromagnetic fields for which metallic mirrors can have an impact, e.g., on the screening of the electron-electron interactions. Eventually, we expect the presented results to apply also in the case of nonmetallic mirrors such as dielectric mirrors.

Note added. Recently, a preprint by J. Li *et al.* [55] appeared which, in a different context, reaches conclusions similar to what discussed in Sec. V B regarding the smallness of the effects of band renormalization in a planar cavity.

ACKNOWLEDGMENTS

We acknowledge discussions with Martin Eckstein, Jiajun Li, Jean-Marc Triscone, Yannis Laplace, Antoine Georges, Daniele Fausti, Alexey Kuzmenko, Daniele De Bernardis, Yanko Todorov, and Atac Imamoglu. This work has been supported by the Swiss National Science Foundation through an AMBIZIONE grant. Part of this work has been supported by the European Research Council (Gran No. ERC-319286-QMAC). I.A. acknowledges hospitality at the Collège de France during the early stages of this project. I. C. acknowledges financial support from the European Union FET-Open Grant MIR-BOSE (No. 737017), the H2020-FETFLAG-2018-2020 project 'PhoQuS' (No. 820392) and from the Provincia Autonoma di Trento, partly through the Q@TN - Quantum Science and Technology in Trento initiative.

APPENDIX: RESPONSE FUNCTIONS

In this Appendix, we provides details of the derivation of Eqs. (13)–(15) for calculations the response functions. The starting point is the partition function $\mathcal{Z}$ written as a functional integral over photonic and electronics degrees of freedom

$$\mathcal{Z} = \int \prod_{Q} \mathcal{D}[\Phi_Q, \Phi_Q^*] \prod_{\mathbf{k}\nu} \mathcal{D}[\Psi_{\mathbf{k}\nu}, \Psi_{\mathbf{k}\nu}^*] e^{-\mathcal{S}[\Phi,\Phi^*,\Psi,\Psi^*]}, \tag{A1}$$

where Φ_Q and Φ_Q^*, with $Q \equiv (\mathbf{q}, q_z, \sigma)$, are pairs of conjugate complex variables, while $\Psi_{\mathbf{k}\nu}$ and $\Psi_{\mathbf{k}\nu}^*$ are pairs of conjugate Grassmann variables. In the following, we will adopt the compact notation for the functional differential $\int \mathcal{D}_\Phi \equiv \int \prod_Q \mathcal{D}[\Phi_Q, \Phi_Q^*]$ and $\int \mathcal{D}_\Psi \equiv \int \prod_{\mathbf{k}\nu} \mathcal{D}[\Psi_{\mathbf{k}\nu}, \Psi_{\mathbf{k}\nu}^*]$ The action $\mathcal{S}$ depends on all the variables and reads

$$\mathcal{S} = \mathcal{S}_{\rm ph}^0[\Phi, \Phi^*] + \mathcal{S}_{\rm el}^0[\Psi, \Psi^*] + \mathcal{S}_{\rm int}[\Phi, \Phi^*, \Psi, \Psi^*], \tag{A2}$$

where $\mathcal{S}_{\rm ph}^0 = -\int_0^\beta d\tau d\tau' \sum_Q \Phi_Q^*(\tau)[D_Q^0(\tau-\tau')]^{-1}\Phi_Q(\tau')$ and $\mathcal{S}_{\rm el}^0 = -\int_0^\beta d\tau d\tau' \sum_{\mathbf{k}\nu} \Psi_{\mathbf{k}\nu}^*(\tau)[\mathcal{G}_{\mathbf{k}\nu}^0(\tau-\tau')]^{-1}\Psi_{\mathbf{k}\nu}(\tau')$ are the non interacting actions with D_Q^0 and $\mathcal{G}_{\mathbf{k}\nu}^0$ the bare photonic and electronic propagators, respectively. The interaction action is split as $\mathcal{S}_{\rm int} = \mathcal{S}_{AP} + \mathcal{S}_{AA}$ with

$$\mathcal{S}_{AP} = \int_0^\beta d\tau H_{AP}[\Phi(\tau), \Phi(\tau)^*, \Psi(\tau), \Psi(\tau)^*] \tag{A3}$$

and

$$\mathcal{S}_{AA} = \int_0^\beta d\tau H_{AA}[\Phi(\tau), \Phi(\tau)^*, \Psi(\tau), \Psi(\tau)^*] \tag{A4}$$

with H_{AP} and H_{AA} the Hamiltonian defined in Eqs. (4) and (5). Thanks to the decoupling Eq. (10) the term $\mathcal{S}_{AA}$ can be absorbed in the non interacting photonic action $\mathcal{S}_{\rm ph}^0$ upon redefining the photonic propagator $D^0 \to \mathcal{D}_0$ with self-energy in Eq. (12). Specifically, after introducing the vectorial representation $\mathbf{\Phi}_Q \equiv \binom{\Phi_Q}{\Phi_{-Q}^*}$, we have

$$\mathcal{S}_{\rm ph}^0 + \mathcal{S}_{AA} \to -\frac{1}{2}\int_0^\beta d\tau d\tau' \sum_{QQ'} \mathbf{\Phi}_Q^\dagger(\tau)[\mathcal{D}_0(\tau-\tau')]_{QQ'}^{-1}\mathbf{\Phi}_{Q'}, \tag{A5}$$

where the photonic propagator is defined as

$$[\mathcal{D}_0(\tau-\tau')]_{QQ'}^{-1} = -\delta(\tau-\tau')(\delta_{QQ'}\overline{\partial}_\tau + \overline{\omega}_{QQ'}), \tag{A6}$$

where $\overline{\omega}_{QQ'}$ are the energy of the modes dressed by the $\mathbf{A}^2$ term via the self-energy Eq. (12) and the symbol

$\overline{\partial}_\tau = \begin{pmatrix} \partial_\tau & 0 \\ 0 & -\partial_\tau \end{pmatrix}$. Notice that upon decoupling of the diamagnetic term there is also a purely electronic term that can be reabsorbed in the noninteracting electronic Hamiltonian. This term enters as a redefinition of the chemical potential and will be discarded.

With the above simplifications the interacting Hamiltonian can be written as

$$\mathcal{S}_{\rm int} = \frac{1}{2}\int d\tau \sum_Q \mathbf{\Gamma}_Q^\dagger(\tau)\mathbf{\Phi}_Q(\tau) + \mathbf{\Phi}_Q^\dagger(\tau)\mathbf{\Gamma}_Q(\tau), \tag{A7}$$

where we introduce the spinors

$$\mathbf{\Gamma}_Q \equiv \begin{pmatrix} \Gamma_Q \\ \Gamma^*_{-Q} \end{pmatrix} = \frac{\gamma_Q}{\sqrt{L}}\begin{pmatrix} 1 \\ 1 \end{pmatrix} \boldsymbol{v}_Q \cdot \mathbf{J}_P(-\mathbf{q}) \tag{A8}$$

with

$$\mathbf{J}_P(\mathbf{q}) = \frac{e}{m}\frac{1}{S}\sum_{\mathbf{k}\nu\nu'} \mathbf{p}^{\mathbf{k}\nu'}_{\mathbf{k}+\mathbf{q}\nu} \Psi^*_{\mathbf{k}+\mathbf{q}\nu}\Psi_{\mathbf{k}\nu'}. \tag{A9}$$

In the compact index notation $-Q \equiv (-\mathbf{q}q_z\sigma)$. By integrating over photonic variables and by using Gaussian integration, we get

$$\mathcal{Z} = \int \mathcal{D}_\Psi e^{-\mathcal{S}_{\rm el}[\Psi,\Psi^*]}\mathcal{Z}_{\rm ph}[\Psi,\Psi^*] \tag{A10}$$

with

$$\mathcal{Z}_{\rm ph}[\Psi,\Psi^*] \equiv \int \mathcal{D}_\Phi e^{-\mathcal{S}^0_{\rm ph} - \frac{1}{2}\int d\tau \sum_Q \mathbf{\Gamma}_Q^\dagger(\tau)\mathbf{\Phi}_Q(\tau) + \mathbf{\Phi}_Q^\dagger(\tau)\mathbf{\Gamma}_Q(\tau)}$$
$$= e^{-\frac{1}{2}\int_0^\beta d\tau d\tau' \sum_{QQ'} \mathbf{\Gamma}_Q^\dagger(\tau)[\mathcal{D}(\tau-\tau')]_{QQ'}\mathbf{\Gamma}_{Q'}(\tau')}. \tag{A11}$$

By taking the functional derivative $\frac{\delta^2}{\delta J^i_P(-\mathbf{q},\tau)\delta J^j_P(\mathbf{q},\tau')}$ of both sides of Eq. (A11) and by integrating over the fermionic variables we arrive, after simple manipulations, at Eq. (13) in the main text with $\chi^{ij}_{PP}(\mathbf{q},\tau-\tau') = \delta_{ij}\chi_{PP}(\mathbf{q},\tau-\tau') = -\langle T_\tau J^i_P(-\mathbf{q},\tau)J^i_P(\mathbf{q},\tau')\rangle$.

The correlation functions involving the diamagnetic contribution to the current are obtained by first applying the diamagnetic decoupling to the diamagnetic current $\mathbf{J}_A = \frac{e^2}{m}\int d\mathbf{x}\rho(\mathbf{x})\mathbf{A}(\mathbf{x})$, with $\rho_0(\mathbf{x})$ the electronic density of the noninteracting system. The mixed correlation function χ_{AP} is therefore obtained by using the equations of motion. Specifically, it is straightforward to check that

$$-\overline{\partial_\tau}\mathbf{\Phi}_Q(\tau) = \sum_{Q'}\overline{\omega}_{QQ'}\Phi_{Q'}(\tau) + \mathbf{\Gamma}_Q \tag{A12}$$

where in the last equation the spinors $\mathbf{\Phi}_Q(\tau)$ and $\mathbf{\Gamma}_Q$ should be considered at the operatorial level. By applying the equation of motion to the correlator $\chi(\mathbf{q},\tau-\tau') = -\langle T_\tau J_A(-\mathbf{q},\tau)J_P(\mathbf{q},\tau')\rangle$ and using the definition of the photon propagator dressed by the $\mathbf{A}^2$ term, Eq. (A6), we arrive at Eq. (14) in the text.

Eventually the purely diamagnetic response χ_{AA} is straightforwardly written in term of the photon propagator by direct expansion of the vector potential operator.

We notice that in all the above steps we have always assumed that the photon propagator keeps the full in-plane translational invariance $\mathcal{D} \sim \delta_{\mathbf{q}\mathbf{q}'}$ as discussed in Sec. III A.

[1] T. W. Ebbesen, Hybrid light-matter states in a molecular and material science perspective, Acc. Chem. Res. **49**, 2403 (2016).

[2] A. Frisk Kockum, A. Miranowicz, S. De Liberato, S. Savasta, and F. Nori, Ultrastrong coupling between light and matter, Nat. Rev. Phys. **1**, 19 (2019).

[3] I. Carusotto and C. Ciuti, Quantum fluids of light, Rev. Mod. Phys. **85**, 299 (2013).

[4] M. A. Sentef, M. Ruggenthaler, and A. Rubio, Cavity quantum-electrodynamical polaritonically enhanced electron-phonon coupling and its influence on superconductivity, Sci. Adv. **4**, eaau6969 (2018).

[5] F. Schlawin, A. Cavalleri, and D. Jaksch, Cavity-Mediated Electron-Photon Superconductivity, Phys. Rev. Lett. **122**, 133602 (2019).

[6] J. B. Curtis, Z. M. Raines, A. A. Allocca, M. Hafezi, and V. M. Galitski, Cavity Quantum Eliashberg Enhancement of Superconductivity, Phys. Rev. Lett. **122**, 167002 (2019).

[7] Y. Ashida, A. İmamoğlu, J. Faist, D. Jaksch, A. Cavalleri, and E. Demler, Quantum Electrodynamic Control of Matter: Cavity-Enhanced Ferroelectric Phase Transition, Phys. Rev. X **10**, 041027 (2020).

[8] A. Chiocchetta, D. Kiese, C. P. Zelle, F. Piazza, and S. Diehl, Cavity-induced quantum spin liquids, Nat. Commun. **12**, 5901 (2021).

[9] A. Thomas, E. Devaux, K. Nagarajan, T. Chervy, M. Seidel, D. Hagenmüller, S. Schütz, J. Schachenmayer, C. Genet, G. Pupillo, and T. W. Ebbesen, Exploring superconductivity under strong coupling with the vacuum electromagnetic field, arXiv:1911.01459.

[10] D. De Bernardis, T. Jaako, and P. Rabl, Cavity quantum electrodynamics in the nonperturbative regime, Phys. Rev. A **97**, 043820 (2018).

[11] M. Schuler, D. D. Bernardis, A. M. Läuchli, and P. Rabl, The Vacua of Dipolar Cavity Quantum Electrodynamics, SciPost Phys. **9**, 66 (2020).

[12] E. Cortese, N.-L. Tran, J.-M. Manceau, A. Bousseksou, I. Carusotto, G. Biasiol, R. Colombelli, and S. De Liberato, Excitons bound by photon exchange, Nat. Phys. **17**, 31 (2021).

[13] G. M. Andolina, F. M. D. Pellegrino, V. Giovannetti, A. H. MacDonald, and M. Polini, Theory of photon condensation in a spatially varying electromagnetic field, Phys. Rev. B **102**, 125137 (2020).

[14] D. Guerci, P. Simon, and C. Mora, Superradiant Phase Transition in Electronic Systems and Emergent Topological Phases, Phys. Rev. Lett. **125**, 257604 (2020).

[15] P. Nataf, T. Champel, G. Blatter, and D. M. Basko, Rashba Cavity Qed: A Route Towards the Superradiant Quantum Phase Transition, Phys. Rev. Lett. **123**, 207402 (2019).

[16] X. Wang, E. Ronca, and M. A. Sentef, Cavity quantum electrodynamical chern insulator: Towards light-induced quantized anomalous hall effect in graphene, Phys. Rev. B **99**, 235156 (2019).

[17] H. Hübener, U. De Giovannini, C. Schäfer, J. Andberger, M. Ruggenthaler, J. Faist, and A. Rubio, Engineering quantum materials with chiral optical cavities, Nat. Mater. **20**, 438 (2021).

[18] M. Kiffner, J. R. Coulthard, F. Schlawin, A. Ardavan, and D. Jaksch, Manipulating quantum materials with quantum light, Phys. Rev. B **99**, 085116 (2019).

[19] J. Li and M. Eckstein, Manipulating Intertwined Orders in Solids with Quantum Light, Phys. Rev. Lett. **125**, 217402 (2020).

[20] D. Nicoletti and A. Cavalleri, Nonlinear light–matter interaction at terahertz frequencies, Adv. Opt. Photon. **8**, 401 (2016).

[21] R. Mankowsky, A. Subedi, M. Forst, S. O. Mariager, M. Chollet, H. T. Lemke, J. S. Robinson, J. M. Glownia, M. P. Minitti, A. Frano, M. Fechner, N. A. Spaldin, T. Loew, B. Keimer, A. Georges, and A. Cavalleri, Nonlinear lattice dynamics as a basis for enhanced superconductivity in $YBa_2Cu_3O_{6.5}$, Nature (London) **516**, 71 (2014).

[22] M. Mitrano, A. Cantaluppi, D. Nicoletti, S. Kaiser, A. Perucchi, S. Lupi, P. Di Pietro, D. Pontiroli, M. Riccò, S. R. Clark, D. Jaksch, and A. Cavalleri, Possible light-induced superconductivity in K_3C_{60} at high temperature, Nature (London) **530**, 461 (2016).

[23] E. T. Jaynes and F. W. Cummings, Comparison of quantum and semiclassical radiation theories with application to the beam maser, Proc. IEEE **51**, 89 (1963).

[24] J. Skolimowski, A. Amaricci, and M. Fabrizio, Misuse of the minimal coupling to the electromagnetic field in quantum many-body systems, Phys. Rev. B **101**, 121104(R) (2020).

[25] Y. Laplace, S. Fernandez-Pena, S. Gariglio, J. M. Triscone, and A. Cavalleri, Proposed cavity Josephson plasmonics with complex-oxide heterostructures, Phys. Rev. B **93**, 075152 (2016).

[26] E. Orgiu, J. George, J. A. Hutchison, E. Devaux, J. F. Dayen, B. Doudin, F. Stellacci, C. Genet, J. Schachenmayer, C. Genes, G. Pupillo, P. Samorì, and T. W. Ebbesen, Conductivity in organic semiconductors hybridized with the vacuum field, Nat. Mater. **14**, 1123 (2015).

[27] D. Hagenmüller, J. Schachenmayer, S. Schütz, C. Genes, and G. Pupillo, Cavity-Enhanced Transport of Charge, Phys. Rev. Lett. **119**, 223601 (2017).

[28] K. Nagarajan, J. George, A. Thomas, E. Devaux, T. Chervy, S. Azzini, K. Joseph, A. Jouaiti, M. W. Hosseini, A. Kumar, C. Genet, N. Bartolo, C. Ciuti, and T. W. Ebbesen, Conductivity and photoconductivity of a p-type organic semiconductor under ultrastrong coupling, ACS Nano **14**, 10219 (2020).

[29] V. Rokaj, M. Ruggenthaler, F. G. Eich, and A. Rubio, The free electron gas in cavity quantum electrodynamics, arXiv:2006.09236.

[30] N. Bartolo and C. Ciuti, Vacuum-dressed cavity magnetotransport of a two-dimensional electron gas, Phys. Rev. B **98**, 205301 (2018).

[31] G. L. Paravicini-Bagliani, F. Appugliese, E. Richter, F. Valmorra, J. Keller, M. Beck, N. Bartolo, C. Rössler, T. Ihn, K. Ensslin, C. Ciuti, G. Scalari, and J. Faist, Magneto-transport controlled by landau polariton states, Nat. Phys. **15**, 186 (2019).

[32] K. Kakazu and Y. S. Kim, Quantization of electromagnetic fields in cavities and spontaneous emission, Phys. Rev. A **50**, 1830 (1994).

[33] Y. Todorov and C. Sirtori, Intersubband polaritons in the electrical dipole gauge, Phys. Rev. B **85**, 045304 (2012).

[34] D. De Bernardis, P. Pilar, T. Jaako, S. De Liberato, and P. Rabl, Breakdown of gauge invariance in ultrastrong-coupling cavity qed, Phys. Rev. A **98**, 053819 (2018).

[35] O. Di Stefano, A. Settineri, V. Macrì, L. Garziano, R. Stassi, S. Savasta, and F. Nori, Resolution of gauge ambiguities in ultrastrong-coupling cavity quantum electrodynamics, Nat. Phys. **15**, 803 (2019).

[36] M. Schüler, J. A. Marks, Y. Murakami, C. Jia, and T. P. Devereaux, Gauge invariance of light-matter interactions in first-principle tight-binding models, Phys. Rev. B **103**, 155409 (2021).

[37] J. Li, D. Golez, G. Mazza, A. J. Millis, A. Georges, and M. Eckstein, Electromagnetic coupling in tight-binding models for strongly correlated light and matter, Phys. Rev. B **101**, 205140 (2020).

[38] Y. Ashida, Ataç İmamoğlu, and E. Demler, Cavity Quantum Electrodynamics at Arbitrary Light-Matter Coupling Strengths, Phys. Rev. Lett. **126**, 153603 (2021).

[39] O. Dmytruk and M. Schiró, Gauge fixing for strongly correlated electrons coupled to quantum light, Phys. Rev. B **103**, 075131 (2021).

[40] C. Ciuti, G. Bastard, and I. Carusotto, Quantum vacuum properties of the intersubband cavity polariton field, Phys. Rev. B **72**, 115303 (2005).

[41] C. Schäfer, M. Ruggenthaler, V. Rokaj, and A. Rubio, Relevance of the quadratic diamagnetic and self-polarization terms in cavity quantum electrodynamics, ACS Photon. **7**, 975 (2020).

[42] K. Rzażewski, K. Wódkiewicz, and W. Żakowicz, Phase Transitions, Two-Level Atoms, and the A^2 Term, Phys. Rev. Lett. **35**, 432 (1975).

[43] G. Mazza and A. Georges, Superradiant Quantum Materials, Phys. Rev. Lett. **122**, 017401 (2019).

[44] G. M. Andolina, F. M. D. Pellegrino, V. Giovannetti, A. H. MacDonald, and M. Polini, Cavity quantum electrodynamics of strongly correlated electron systems: A no-go theorem for photon condensation, Phys. Rev. B **100**, 121109(R) (2019).

[45] E. Cortese, I. Carusotto, R. Colombelli, and S. De Liberato, Strong coupling of ionizing transitions, Optica **6**, 354 (2019).

[46] K. Mak and J. Shan, Photonics and optoelectronics of 2d semiconductor transition metal dichalcogenides, Nat. Photon. **10**, 216 (2016).

[47] X. Liu, T. Galfsky, Z. Sun, F. Xia, E.-C. Lin, Y.-H. Lee, S. Kéna-Cohen, and V. M. Menon, Strong light–matter coupling in two-dimensional atomic crystals, Nat. Photon. **9**, 30 (2014).

[48] S. Latini, E. Ronca, U. De Giovannini, H. Hübener, and A. Rubio, Cavity control of excitons in two-dimensional materials, Nano Lett. **19**, 3473 (2019).

[49] H. A. Bethe, The electromagnetic shift of energy levels, Phys. Rev. **72**, 339 (1947).

[50] P.-B. Vigneron, S. Pirotta, I. Carusotto, N.-L. Tran, G. Biasiol, J.-M. Manceau, A. Bousseksou, and R. Colombelli, Quantum well infrared photo-detectors operating in the strong light-matter coupling regime, Appl. Phys. Lett. **114**, 131104 (2019).

[51] S. De Liberato and C. Ciuti, Quantum theory of electron tunneling into intersubband cavity polariton states, Phys. Rev. B **79**, 075317 (2009).

[52] S. De Liberato and C. Ciuti, Quantum model of microcavity intersubband electroluminescent devices, Phys. Rev. B **77**, 155321 (2008).

[53] J. Dubail, T. Botzung, J. Schachenmayer, G. Pupillo, and D. Hagenmüller, Large random arrowhead matrices: Multifractality, semi-localization, and protected transport in disordered quantum spins coupled to a cavity, arXiv:2105.08444.

[54] T. Botzung, D. Hagenmüller, S. Schütz, J. Dubail, G. Pupillo, and J. Schachenmayer, Dark state semilocalization of quantum emitters in a cavity, Phys. Rev. B **102**, 144202 (2020).

[55] J. Li, L. Schamriß, and M. Eckstein, Effective theory of lattice electrons strongly coupled to quantum electromagnetic fields, arXiv:2105.08711.